The Principle of Maximum Chiral Discrimination: Chiral Recognition in Permethyl-β-cyclodextrin

Kenny B. Lipkowitz,* Robert Coner,† Michael A. Peterson,‡ Antonio Morreale, and Jason Shackelford

Department of Chemistry, Indiana University−Purdue University at Indianapolis (IUPUI), 402 North Blackford Street, Indianapolis, Indiana 46202

Received September 12, 1997

Five guest molecules, isomenthone, pulegone, 1-fluoro-1-phenylethane, 1-phenylethanol, and 2-methylbutanoic acid, binding to permethyl-β-cyclodextrin, a chiral host molecule, have been simulated by molecular dynamics techniques. From the simulations we find the preferred binding site to be the interior of the macrocyclic cavity. A new technique was used for locating the host's most enantiodiscriminating domain, which was also found to be inside the macrocyclic cavity. It is concluded that this particular host molecule displays its enhanced chiral discriminating capacity because of this spatial coincidence. Also evaluated in this paper are the types and magnitudes of intermolecular forces responsible for diastereomeric complexation and chiral discrimination; in both cases the short-range dispersion forces dominate. This study illustrates the "principle of maximum chiral recognition", the idea that maximum chiral recognition can be achieved by maintaining a spatial congruence between the host's domain of greatest enantiodifferentiation with the guest's preferred binding site.

Introduction

There has been a remarkable infusion of cyclodextrin-assisted studies into the chemical sciences during the last three decades.[1] Concurrent with this has been the use of cyclodextrins (CD) in technology.[2] One especially important application of cyclodextrin technology, for example, has been in the area of separation science.[3] These host molecules have been extensively used for separations because they offer the possibility of coordinating guests of differing size (depending on which CD macrocycle is used), because of their ability to recognize different guest functional groups (depending on which CD derivative is employed), and most significantly, since they are derived from glucose units, these macrocycles are inherently dissymmetric and are thus able to distinguish between stereochemical isomers including enantiomers. The versatility of these macrocycles is remarkable, and because of their price-to-performance ratio they are extensively used in chiral chromatography.[4] Both native and derivatized cyclodextrins have been used to separate enantiomers in planar chromatography (TLC),[5] high-performance liquid chromatography (HPLC),[6] in super- and subcritical fluid-phase chromatographies, and more recently, as additives that enantioselectively bind and control the migratory aptitudes of analytes in capillary electrophoresis.[7] Another area of chromatographic application of cyclodextrins is in gas−liquid-phase chromatography (GLC).[8] Here, analyses of volatile natural and nonnatural products have been undertaken in disciplines as disparate as

Table 1. MD Results (kJ/mol) for Isomenthone/CD

	total	stretch	bend	torsion	vdW	elect
RR1	2031.99	387.65	604.42	525.93	38.03	475.97
RR2	2053.27	389.62	613.65	509.29	65.62	475.09
RR3	2042.79	388.26	608.65	523.18	47.45	475.25
RR4	2069.09	388.14	608.19	526.81	68.59	477.36
RR5	2029.95	387.84	602.46	526.24	36.94	476.47
avg E_{RR}	**2045.42**	**388.30**	**607.47**	**522.29**	**51.32**	**476.03**
SS1	2061.01	388.36	608.17	524.21	62.46	477.81
SS2	2038.96	388.43	608.18	521.60	47.31	473.44
SS3	2035.29	387.71	603.75	530.23	38.50	475.10
SS4	2059.38	388.48	605.41	523.73	64.42	477.34
SS5	2029.23	387.55	603.88	525.15	36.72	475.93
avg E_{SS}	**2044.77**	**388.11**	**605.88**	**524.98**	**49.88**	**475.92**
$\overline{\Delta\Delta E_{R-S}}$	**0.64**	**0.20**	**1.60**	**−2.69**	**1.44**	**0.10**

* To whom correspondence should be addressed. E-mail: lipkowitz@chem.iupui.edu.

† Permanent address: Lilly Research Laboratories, Lilly Corporate Center, Drop 0540, Indianapolis, IN 46285.

‡ Permanent address: Department of Chemistry, University of Florida, Box 117200, Gainesville, FL 32611-7200.

(1) (a) Bender, M. L.; Komiyama, M. *Cyclodextrin Chemistry, Reactivity and Structure, Concepts in Organic Chemistry, 6*; Springer-Verlag: New York, 1978. (b) Saenger, W. *Angew. Chem., Int. Ed. Engl.*, **1980**, *19*, 344. (c) Szejtli, J. *Cyclodextrins and Their Inclusion Complexes*; Akadémiai Kaidó: Budapest, 1982.

(2) (a) Duchêne, D., Ed. *Cyclodextrins and Their Industrial Uses*; Editions de Sante: Paris, 1987. (b) Szejtli, J. *Cyclodextrin Technology*; Kluwer Academic: Dordrecht, 1988.

(3) Snopek, J.; Smolková-Keulemansová, E.; Cserháti, T.; Gahm, K. H.; Stalcup, A. In *Comprehensive Supramolecular Chemistry*; Szejtli, J., Osa, T., Eds.; Pergamon Press: Oxford, 1996; pp 515−571.

(4) (a) Souter, R. W. *Chromatographic Separations of Stereoisomers*; CRC Press: Boca Raton, 1985. (b) *Chromatographic Chiral Separations*; Zeif, M., Crane, L., Eds.; Chromatographic Science Series, Vol. 40; Marcel Dekker: New York, 1987. (c) König, W. A. *The Practice of Enantiomer Separation by Capillary Gas Chromatography*; Hüthig: Heidelberg, 1987. (d) *Ordered Media in Chemical Separations*; Hinze, W. L., Armstrong, D. W., Eds.; ACS Symposium Series 342; American Chemical Society: Washington, DC, 1987. (e) Allenmark, S. G. *Chromatographic Enantioseparation. Methods and Application*; Ellis Horwood: Chichester, 1988. (f) *Chiral Separations*; Stevenson, D., Wilson, I. D., Eds.; Plenum: New York, 1988. (g) *Chiral Liquid Chromatography*; Lough, W. J., Ed.; Blackie: London, 1989. (h) *Recent Advances in Chiral Separations*; Stevenson, D., Wilson, I. D., Eds.; Plenum: New York, 1990. (i) *Chiral Separations by Liquid Chromatography*; Ahuja, S., Ed.; ACS Symposium Series 471; American Chemical Society: Washington, DC, 1991. (j) *Chiral Separations by Liquid Chromatography*; Subramanian, G., Ed.; VCH: Weinheim, 1994. (k) *Chiral Separations. Applications and Technology*; Ahuja, S., Ed.; American Chemical Society: Washington, DC, 1997.

(5) For reviews see: (a) Ward, T. J.; Armstrong, D. W. *J. Liq. Chromatogr.* **1986**, *9*, 407. (b) Martens, J.; Bhushan, R. *Chem. Ztg.* **1988**, *112*, 367. (c) Martens, J.; Bhushan, R. *Int. J. Peptide Protein Res.* **1989**, *34*, 433. (d) Martens, J.; Bhushan, R. *J. Pharm. Biomed. Anal.* **1990**, *8*, 259. (e) Bhushan, R.; Joshi, S. *Biomed. Chromatogr.* **1993**, *7*, 235.

S0022-3263(97)01709-X CCC: $15.00
Published on Web 01/22/1998

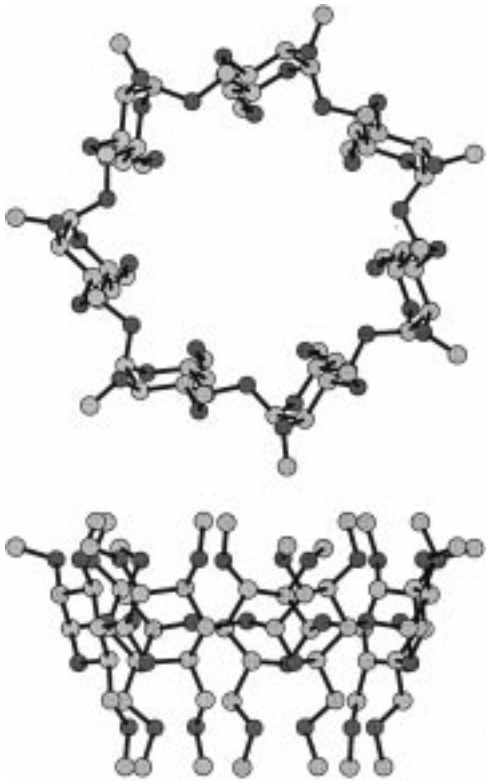

Figure 1. (Top) view looking into the permethyl-β-cyclodextrin chiral cavity. (Bottom) side view illustrating the typical conical shape of these molecules. The more open end on top is designated the secondary rim and the narrower end on the bottom is the primary rim because it once had primary hydroxyl groups before alkylation. These views are what one would expect to see using a slow spectral technique like NMR spectroscopy. These molecules tend to undergo wide amplitude fluctuations and at any given time are distorted from 7-fold symmetry. Dark gray tones represent oxygen atoms and light gray tones are carbons. Hydrogen atoms omitted for clarity.

Table 2. MD Results (kJ/mol) for Pulegone/CD

	total	stretch	bend	torsion	vdW	elect
R1	2118.64	416.85	644.53	544.26	65.36	447.64
R2	2112.79	416.27	641.31	547.01	61.40	446.79
R3	2126.26	417.33	651.10	540.74	77.40	439.69
R4	2118.25	417.68	652.61	532.53	73.03	442.40
R5	2118.13	417.80	652.55	527.37	75.06	445.34
avg E_R	**2118.81**	**417.19**	**648.42**	**538.38**	**70.45**	**444.37**
S1	2114.78	417.23	648.23	533.96	72.90	442.46
S2	2113.55	416.68	645.76	542.67	62.09	446.36
S3	2119.81	417.55	650.97	529.47	76.52	445.30
S4	2113.30	417.17	647.21	536.51	67.16	445.25
S5	2119.57	416.27	644.29	546.84	67.03	445.14
avg E_S	**2116.20**	**416.98**	**647.29**	**537.89**	**69.14**	**444.90**
$\overline{\Delta\Delta E_{R-S}}$	**2.61**	**0.21**	**1.13**	**0.49**	**1.31**	**−0.53**

physical organic chemistry,[9] geochemistry,[10] and pheromone research[11] as well as in the aromas,[12] fragrances,[13] and food additives business.[14] Cyclodextrins, both in their native and derivatized forms, have thus clearly established themselves as a mainstay for chiral resolutions and are prototypical host−guest complexing agents that have been used by many researchers whose studies have focused on aspects of molecular recognition.

Despite these well-established technological applications and exhaustive scientific studies, one of the questions many scientists still pose is: "How do they work?" In this paper, we address that general question by decomposing it into the following four key questions, each of which will be answered through molecular simulation.

(1) Where in or around the macrocycle do analytes tend to bind? This is a particularly important question to ad-

Table 3. MD Results (kJ/mol) for 1-Fluorophenylethane/CD

	total	stretch	bend	torsion	vdW	elect
R1	1904.63	369.67	566.61	510.56	31.84	425.95
R2	1903.98	369.75	566.04	511.17	21.98	427.04
R3	1918.67	370.76	572.73	500.32	50.83	424.03
R4	1924.43	370.17	569.47	509.52	48.81	426.46
R5	1920.68	369.70	568.05	510.07	46.48	426.38
avg E_R	**1912.93**	**370.01**	**568.58**	**508.33**	**41.59**	**425.97**
S1	1904.18	369.49	565.24	511.46	30.79	427.70
S2	1917.63	370.65	571.97	500.75	50.52	423.79
S3	1905.39	369.76	567.58	510.69	31.69	425.67
S4	1926.71	370.23	569.74	509.44	48.82	428.48
S5	1906.38	369.06	564.39	512.20	33.08	427.65
avg E_S	**1913.49**	**369.84**	**567.78**	**508.91**	**38.98**	**426.56**
$\overline{\Delta\Delta E_{R-S}}$	**−0.56**	**0.17**	**0.80**	**−0.58**	**2.61**	**−0.59**

Table 4. MD Results (kJ/mol) for 1-Phenylethanol/CD

	total	stretch	bend	torsion	vdW	elect
R1	1972.82	396.15	602.55	516.44	42.36	415.32
R2	1985.65	397.42	612.16	501.76	62.97	411.34
R3	1983.59	397.13	611.06	505.41	57.99	412.00
R4	1975.31	396.55	606.22	516.50	42.41	413.63
R5	1965.03	396.18	605.01	517.21	34.60	412.03
avg E_R	**1976.42**	**396.69**	**607.40**	**511.46**	**48.07**	**412.86**
S1	1979.34	396.55	604.90	517.42	46.96	413.51
S2	1968.16	396.43	606.33	516.84	36.68	411.88
S3	1973.52	397.35	608.55	505.56	48.28	413.78
S4	1992.69	397.54	611.03	505.51	65.86	412.75
S5	1963.82	396.16	603.08	518.47	33.47	412.64
avg E_S	**1975.51**	**396.81**	**606.78**	**512.76**	**46.25**	**412.91**
$\overline{\Delta\Delta E_{R-S}}$	**0.97**	**−0.12**	**0.62**	**−1.30**	**1.82**	**0.05**

Table 5. MD Results (kJ/mol) for 2-Methylbutanoic Acid/CD

	total	stretch	bend	torsion	vdW	elect
R1	1922.13	393.74	617.95	498.10	51.24	361.10
R2	1926.97	393.53	614.31	506.94	46.09	366.10
R3	1927.44	392.73	612.95	503.83	44.27	373.66
R4	1917.53	392.15	606.54	511.03	33.73	374.08
R5	1924.47	393.12	614.21	497.73	49.46	369.95
avg E_R	**1923.71**	**393.05**	**613.19**	**503.53**	**44.96**	**368.98**
S1	1920.88	393.19	611.32	502.34	43.00	371.03
S2	1919.82	393.09	608.54	508.01	38.41	371.77
S3	1924.52	393.32	613.91	499.62	47.32	370.35
S4	1929.35	392.56	611.05	507.48	46.18	372.08
S5	1928.14	393.28	614.78	498.89	49.14	372.05
avg E_S	**1924.54**	**393.09**	**611.92**	**503.27**	**44.81**	**371.46**
$\overline{\Delta\Delta E_{R-S}}$	**−0.83**	**−0.03**	**1.27**	**0.26**	**0.15**	**−2.48**

(6) Pertinent discussions can be found throughout ref 4; for additional reviews concerning applications of cyclodextrins see: (a) Armstrong, D. W.; Alak, A.; Bui, K.; DeMond, W.; Ward, T.; Riehl, T. E.; Hinze, W. L. *J. Inclusion Phenom.* **1984**, *2*, 533. (b) Armstrong, D. W. *J. Liq. Chromatogr.* **1984**, *7*, 353. (c) Beesley, T. E. *Am. Lab.*, **1985**, May, 78. (d) Ward, T. J.; Armstrong, D. W. *J. Liq. Chromatogr.* **1986**, *9*, 407. (e) Armstrong, D. W.; Han, S. *CRC Crit. Rev. Anal. Chem.*, **1988**, *19*, 175. (f) Johns, D. *Am. Lab.* **1987**, January, 72. (g) Armstrong, D. W. *Anal. Chem.* **1987**, *59*, 84. (h) Pettersson, C. *Trends Anal. Chem.*, **1988**, *7*, 209. (i) Armstrong, D. W.; Hilton, M.; Coffin, L. *LC−GC* **1991**, September, 646. (j) Husain, N.; Warner, I. M. *Am. Lab.* **1993**, October, 80.

(7) For reviews see: (a) Vespalec, R.; Bocek, P. *Electrophoresis* **1994**, *15*, 755. (b) Nishi, H.; Terabe, S. *J. Chromatogr. A* **1995**, *694*, 246. (c) Guttman, A.; Brunet, S.; Cooke, N. *LC−GC* **1996**, January, 14, 32.

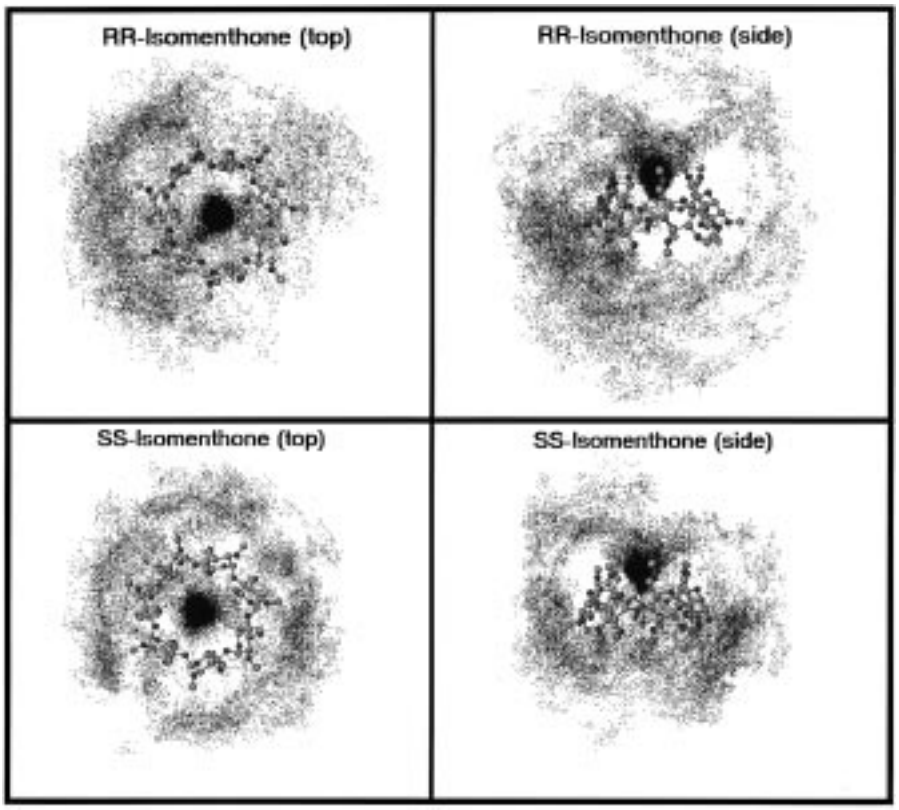

Figure 2. "Dot plot" illustrating the center of mass of guest **2**, relative to the cyclodextrin, over the combined 25 ns simulation. Top: end-on and side views of the *RR* enantiomer. Bottom: end-on and side views of the *SS* enantiomer. Original diagrams are also color coded to indicate the intermolecular energy at each point. Lowest energies are at the interior.

dress because most host−guest studies of cyclodextrins have been carried out in very polar media like water. In those cases, the hydrophobic effect is a dominant driving force for inclusion complexation. While the cyclodextrin-based CSPs used in gas chromatography are often dissolved in a moderately polar medium, there is no hydrophobic force per se and it is not clear if analytes prefer to bind to the interior of the macrocycle or to the exterior of the macrocycle. This controversial issue has been brought to light experimentally by Berthod, Li, and Armstrong,[15] who provided compelling evidence for both interior and exterior binding based on an extrathermodynamic study of a large and diverse set of analytes. Related to this question is whether the analyte prefers to bind to the wider secondary rim, as found in many examples of aqueous guest binding from NMR measurements,[16] at the narrower primary rim, or perhaps somewhere in between.

(2) What are the intermolecular forces holding the complexes together? Are these forces predominantly weak van der Waals forces or more powerful electrostatic forces? Moreover, what percent of the interaction energy can be attributed to each?

(3) What intermolecular forces are most responsible for chiral recognition? Are these the same forces that hold the complexes together or are they different? What percent of the total enantiodifferentiation can be attributed to the short-range dispersion forces and what percent come from the long-range electrical interactions?

(8) Pertinent discussions can be found in ref 4; for additional reviews concerning applications of cyclodextrins in gas chromatography see: (a) Armstrong, D. W.; Han, S. *CRC Crit. Rev. Anal. Chem.* **1988**, *19*, 175. (b) König, W. A. In *Drug Stereochemistry, Analytical Methods and Pharmacology*; Wainer, I. W., Drayer, D. E., Eds.; Marcel Dekker: New York, 1988; pp 113−145. (c) Schurig, V.; Nowotny, H.-P. *Angew. Chem., Int. Ed. Engl.* **1990**, *29*, 939. (d) Jung, M.; Mayer, S.; Schurig, V. *LC−-GC* **1994**, June, 458. (e) Mani, V.; Wooley, C. *Ibid.* **1995**, September, 734.

(9) (a) Enders, D.; Gatzweiler, W.; Dederichs, E. *Tetrahedron* **1990**, *46*, 4757. (b) Baldwin, J. E.; Bonacorsi, S., Jr. *J. Am. Chem. Soc.* **1993**, *115*, 10621. (c) Schurig, V.; Glausch, A.; Fluck, M. *Tetrahedron: Asymmetry* **1995**, *6*, 2161. (d) Asuncion, L.; Baldwin, J. E. *J. Org. Chem.* **1995**, *60*, 5778.

(10) Armstrong, D. W.; Tang, Y.; Zukowski, J. *Anal. Chem.* **1991**, *63*, 2858.

(11) (a) Fletcher, M. T.; Jacobs, M. F.; Kitching, W.; Krohn, S.; Drew, R. A. I.; Haniotakis, G. E.; Francke, W. *J. Chem. Soc., Chem. Commun.* **1992**, 1457. (b) König, W. A.; Gehrcke, B.; Peter, M. G.; Prestwich, G. D. *Tetrahedron: Asymmetry* **1993**, *4*, 165.

(12) (a) Bruche, G.; Dietrich, A.; Mosandl, A. *J. High Resolut. Chromatogr.* **1993**, *16*, 101. (b) Sybilska, D.; Asztemborska, M.; Kowalczyk, J.; Ochocka, R. J.; Ossicini, L.; Perez, G. *J. Chromatogr. A* **1994**, *659*, 389. (c) Reinhardt, R.; Steinborn, A.; Engewald, W.; Anhalt, K.; Schulze, K. *Ibid.* **1995**, *697*, 475. (d) Steinborn, A.; Reinhardt, R.; Engewald, W.; Wyssuwa, K.; Schulze, K. *Ibid.* **1995**, *697*, 485.

(13) (a) Marner, F.-J.; Runge, T.; König, W. A. *Helv. Chim. Acta* **1990**, *73*, 2165. (b) Askari, C.; Hener, U.; Schmarr, H.-G.; Rapp, A.; Mosandl, A. *Fresenius J. Anal. Chem.* **1991**, *340*, 768. (c) Köpke, T.; Mosandl, A. *Z. Lebensm. Unters. Forsch.* **1992**, *194*, 372.

(14) (a) Mosandl, A.; Hollnagel, A. *Chirality* **1989**, *1*, 293. (b) König, W. A.; Evers, P.; Krebber, R.; Schulz, S.; Fehr, C.; Ohloff, G. *Tetrahedron* **1989**, *45*, 7006. (c) Mosandl, A.; Rettinger, K.; Fischer, K.; Schubert, V.; Schmarr, H.-G.; Maas, B. *J. High Resolut. Chromatogr.* **1990**, *13*, 382. (d) Mosandl, A.; Bruche, G.; Askari, C.; Schmarr, H.-G. *Ibid*, **1990**, *13*, 660. (e) Mosandl, A.; Fischer, K.; Hener, U.; Kreis, P.; Rettinger, K.; Schubert, V.; Schmarr, H.-G. *J. Agric. Food Chem.* **1991**, *39*, 1131. (f) Askari, C.; Mosandl, A. *Phytochem. Anal.* **1991**, *2*, 211. (g) Köpke, T.; Schmarr, H.-G.; Mosandl, A. *Flavor Fragr. J.*, **1992**, *7*, 205. (h) Bruche, G.; Mosandl, A.; Kinkel, J. N. *J. High Resolut. Chromatogr.* **1993**, *16*, 254. (i) Karl, V.; Gutser, J.; Dietrich, A.; Maas, B.; Mosandl, A. *Chirality* **1994**, *6*, 427.

(15) Berthod, A.; Li, W.; Armstrong, D. W. *Anal. Chem.* **1992**, *64*, 873.

(16) Schneider, H.-J.; Ikeda, H. *Chem. Rev.* **1997**, in press.

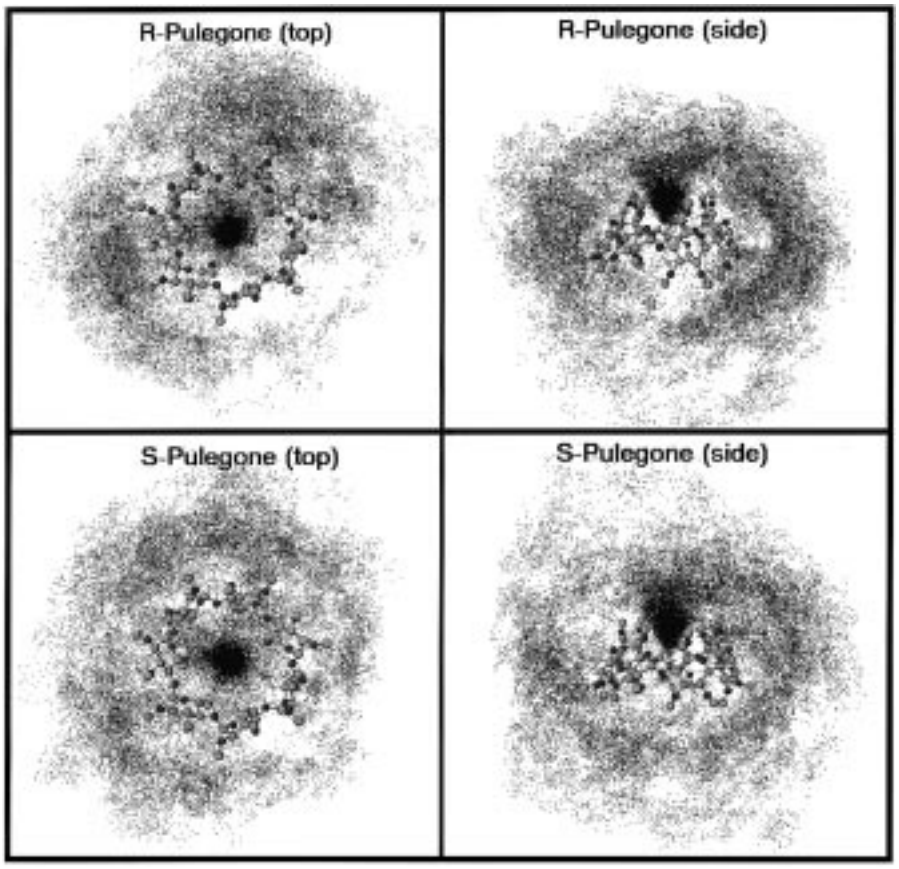

Figure 3. "Dot plot" illustrating the center of mass of guest **3** relative to the cyclodextrin, over the combined 25 ns simulation. Top: end-on and side views of the *R* enantiomer. Bottom: end-on and side views of the *S* enantiomer. Original diagrams are also color coded to indicate the intermolecular energy at each point. Lowest energies are at the interior.

(4) What regions around the CSP are inherently most enantiodiscriminating? Although the entire cyclodextrin is chiral, there probably exist regions in or around the cyclodextrin that better discriminate between enantiomers than do other regions. This is an especially important but overlooked aspect of chiral discrimination. If, for example, the preferred binding site of a cyclodextrin is the interior of the cavity, but the most discriminating region is on the exterior of the cyclodextrin, one may see a diminished ability in chiral discrimination. Related to this, then, is the question: Are the guest binding domains and the regions of maximum enantiodiscrimination spatially coincident?

Although the focus of these questions is on permethylated β-cyclodextrin (Figure 1) because of its popularity in gas chromatography, the underlying physical principles, in addition to the new concepts being developed here, are directly applicable to any area of organic chemistry where chiral recognition is important.

Below we present the results from molecular dynamics simulations of five pairs of enantiomers binding to permethyl-β-cyclodextrin, **1**. These guest molecules include the following: isomenthone,[17] **2**, pulegone,[18] **3**, 1-fluorophenylethane,[19] **4**, 1-phenylethanol,[19] **5**, and 2-methylbutanoic acid,[20] **6**, each of which have been resolved by **1** that was used as a chiral stationary phase (CSP) in the above-cited gas chromatographic resolutions. These guest molecules contain low to moderately polar functional groups (compounds **2** and **3**), weakly polar (compound **4**), and polar protic functional groups (**5** and **6**), providing a diverse but representative set of analytes typically separated on this popular CSP. Of particular interest are the structurally related phenylethanes **4** and **5**. While the *S* enantiomer of **5** is retained longer on **1**, the order is reversed for **4** where the *R* enantiomer is retained longer. This is not an artifact of changing Cahn–Ingold–Prelog nomenclature, but rather is based on differences in intermolecular associations between guest and host that we can reproduce by simulation (vide infra).

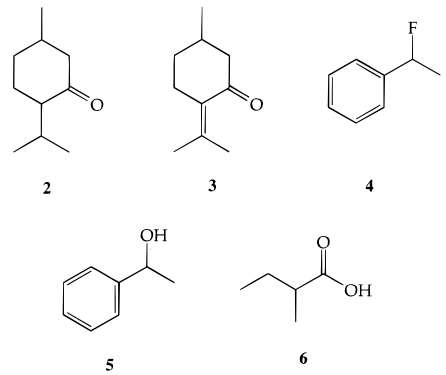

2 3 4 5 6

Simulation Strategy

Under laboratory conditions, analyte molecules are swept through the chromatographic column and interact

(17) Askari, C.; Kreis, P.; Mosandl, A.; Schmarr, H. *Arch. Pharm. (Weinheim)* **1992**, *325*, 35.
(18) Köpke, T.; Mosandl, A. *Z. Lebensm. Unters. Forsch.* **1992**, *194*, 372.
(19) Engwald, W. *Chromatographia* **1994**, 39.
(20) Mosandl, A.; Rettinger, K.; Fischer, K.; Schubert, V.; Schmarr, H.; Maas, B. *J. High Resol. Chromatogr.* **1990**, *13*, 382.

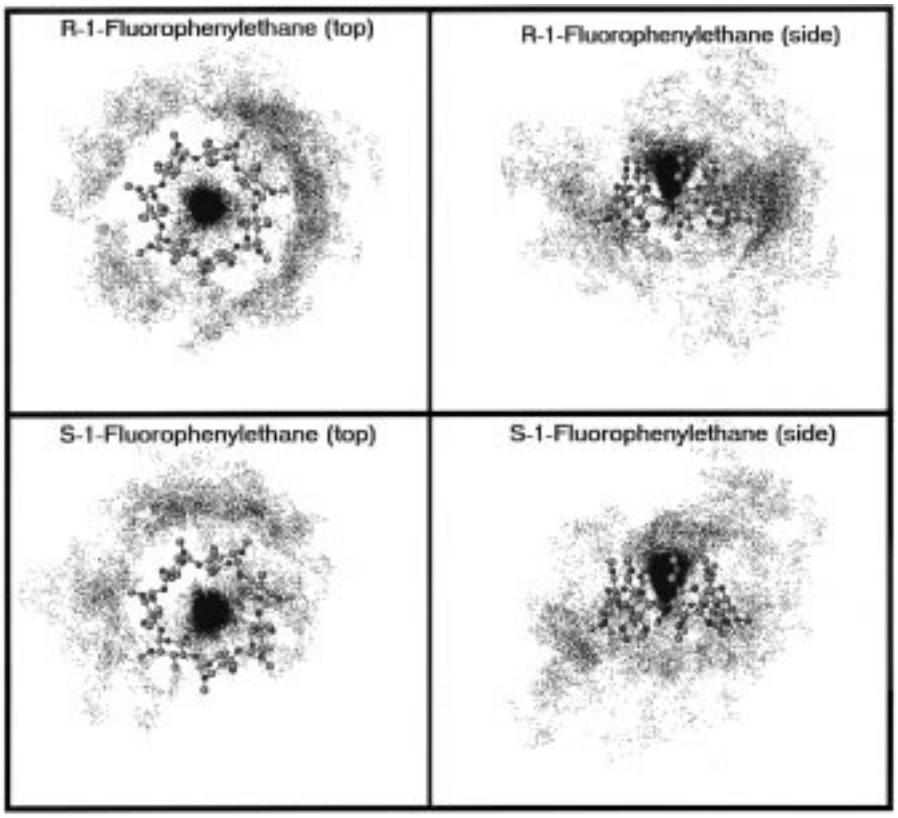

Figure 4. "Dot plot" illustrating the center of mass of guest **4**, relative to the cyclodextrin, over the combined 25 ns simulation. Top: end-on and side views of the *R* enantiomer. Bottom: end-on and side views of the *S* enantiomer. Original diagrams are also color coded to indicate the intermolecular energy at each point. Lowest energies are at the interior.

in a random way with cyclodextrin molecules they encounter during their transit. It would be appropriate to model this situation in its entirety, but this is not possible with existing computing machinery. Instead, we strip the simulation down to its most relevant parts: a host and a guest interacting in a dynamical way. The approach we take is to use a single CSP molecule with a single analyte molecule and carry out stochastic molecular dynamics simulations[21] on those systems. To effect this simulation with a single selector complexing a single selectand, we allow the molecules to bind, dissociate, and rebind multiple times by placing a reflective wall around each diastereomeric complex. To accomplish this, we use a flat-bottom potential having no restraining forces until the analyte molecule moves 20 Å from the cyclodextrin. At that point, a 100 kJ/mol/Å restraining force is applied that pulls the analyte back toward the CSP where it can further associate. Effectively, then, what we've accomplished this way is to allow the analyte to randomly collide with the CSP in all possible conformations, orientations, and positions as it would in the real system.

To probe the system fully we need to sample as large a volume of phase space for each diastereomeric complex as possible. Moreover, to ensure no computational artifacts are introduced into the system, e.g., starting the *R* enantiomer's trajectory on one rim of the cavity and the *S* enantiomer's on the other rim or one enantiomer inside the cavity with the other on the outside, we initially superimpose selected atoms of each enantiomer to generate a racemic "supermolecule" that is then placed in specified starting positions in and around the cyclodextrin. Once both enantiomers have been docked in the same place and with the same orientations/conformations, one of the enantiomers is removed, leaving behind a well-defined binary, diastereomeric complex with the desired stereochemistry.

Five trajectories are run for each enantiomer beginning from five arbitrarily selected initial positions. For docking purposes the cyclodextrin used is a 7-fold symmetric structure that allows us to place the analytes at precise positions parallel or perpendicular to the 7-fold axis. The reader is to note that cyclodextrins are not symmetric at any given time. They are inherently flexible and undergo wide-amplitude flexing motions.[22] Over a long enough simulation time, however, the time-averaged CD structure is expected, and found, to be nearly symmetric. The symmetric structure is used only for docking purposes.

The upshot of our simulation strategy is to sample a wide volume of phase space beginning from different initial conditions corresponding to different locations on the complexes' potential hypersurface. We then run very long simulations (5 ns for *each* trajectory), generating an ensemble of trajectories whose energies are then averaged. This computational protocol has been described in detail in a paper comparing and contrasting rigid-body Monte Carlo simulations with flexible molecular dynamics simulations.[23] The MD simulations were shown in that paper to fully reproduce host−guest binding energies and is de facto the computational protocol used in this study.

(21) van Gunsteren, W. F.; Berendsen, H. J. C. *Mol. Sim.* **1988**, *1*, 173.

(22) Lipkowitz, K. B. *J. Org. Chem.* **1991**, *56*, 6357.

(23) Lipkowitz, K. B.; Pearl, G.; Coner, B.; Peterson. M. A. *J. Am. Chem. Soc.* **1997**, *119*, 600.

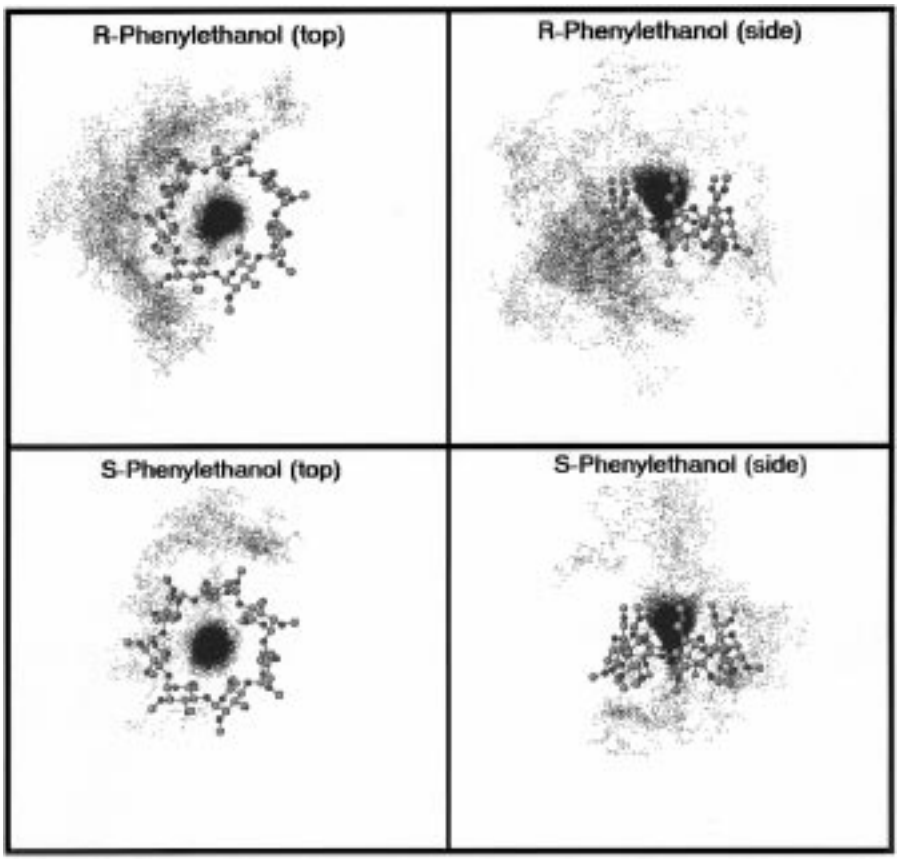

Figure 5. "Dot plot" illustrating the center of mass of guest **5**, relative to the cyclodextrin, over the combined 50 ns simulation. Top: end-on and side views of the *R* enantiomer. Bottom: end-on and side views of the *S* enantiomer. Original diagrams are also color coded to indicate the intermolecular energy at each point. Lowest energies are at the interior.

Table 6. Trajectory-Averaged Intermolecular Energies for 2/CD

	RR		*SS*	
trajectory	vdW	elec	vdW	elec
I	−36.47	−6.02	−12.68	−3.04
II	−8.85	−3.48	−27.42	−6.48
III	−27.84	−4.22	−37.32	−6.71
IV	−7.49	−2.65	−10.34	−4.64
V	−37.96	−6.21	−37.92	−7.32
avg	**−23.68**	**−4.52**	**−25.14**	**−5.64**

Table 7. Trajectory-Averaged Intermolecular Energies for 3/CD

	R		*S*	
trajectory	vdW	elec	vdW	elec
I	−19.16	−1.84	−11.39	−1.28
II	−23.05	−2.06	−23.27	−1.47
III	−8.16	−1.47	−8.00	−1.08
IV	−11.67	−1.43	−17.41	−1.66
V	−11.55	−4.68	−18.64	−1.84
avg	**−14.72**	**−1.74**	**−15.74**	**−1.47**

Computational Tools

All molecular mechanics and molecular dynamics calculations were carried out with the AMBER* force field as found in Macromodel 5.5.[24] The PR conjugate gradient minimizer was used to minimize the energies, and convergence was obtained when the gradient root mean square was below 10^{-3} kJ/mol/Å. Throughout this paper, all force field calculations assume a dielectric of 1.0, and no cutoffs of any kind were used.

Stochastic dynamics (SD) simulations were carried out beginning from the fully optimized lowest-energy molecular mechanics structure. The guest/CD complexes were warmed to the simulation temperature over a period of 5 ps and then equilibrated for 25 ps. During the production simulations of 5000 ps each, structures were saved to disk every 0.5 ps, resulting in 10 000 saved structures from each trajectory. The SD simulation each had a time step of 0.5 fs with equilibration and production run temperatures of 353 K (analyte **2**), 383 K (analyte **3**), 353 K (analyte **4**), 353 K (analyte **5**), and 423 K (analyte **6**) to be consistent with experimental gas chromatography conditions. Translational and rotational momentums were removed every 100 time steps. To keep the CD/guest complexes together, flat-bottom restraints were used between the stereogenic center of the guest molecule and the linking acetal oxygens of the CD. Using these restraints, if the guest strayed more than 20 Å away from any linking acetal oxygen, it was gently pushed back toward the CD. These restraints were used in the heating, equilibration, and production portions of the simulations.

Post-simulation analysis of the SD trajectories was performed with an in-house program called *anout*[25] that computes, among other things, intermolecular energies (using the AMBER* force field in this case) and the center of mass positions of a molecule relative to another. In this work, the guest's positions were calculated relative to the centroid of the best-fit plane through the acetal linking oxygens of the CD. For trajectories being averaged, these guest occurrences were

(24) Mohamadi, F.; Richards, N. G. J.; Guida, W. C.; Liskamp, R.; Caufield, C.; Chang, G.; Hendrickson, T.; Still, W. C. *J. Comput. Chem.* **1990**, *11*, 440.

(25) ANOUT: written by M.A.P. to analyze MacroModel molecular dynamics trajectories. This software is available from Dr. Michael A. Peterson, Department of Chemistry, University of Florida, Gainesville, FL 32611.

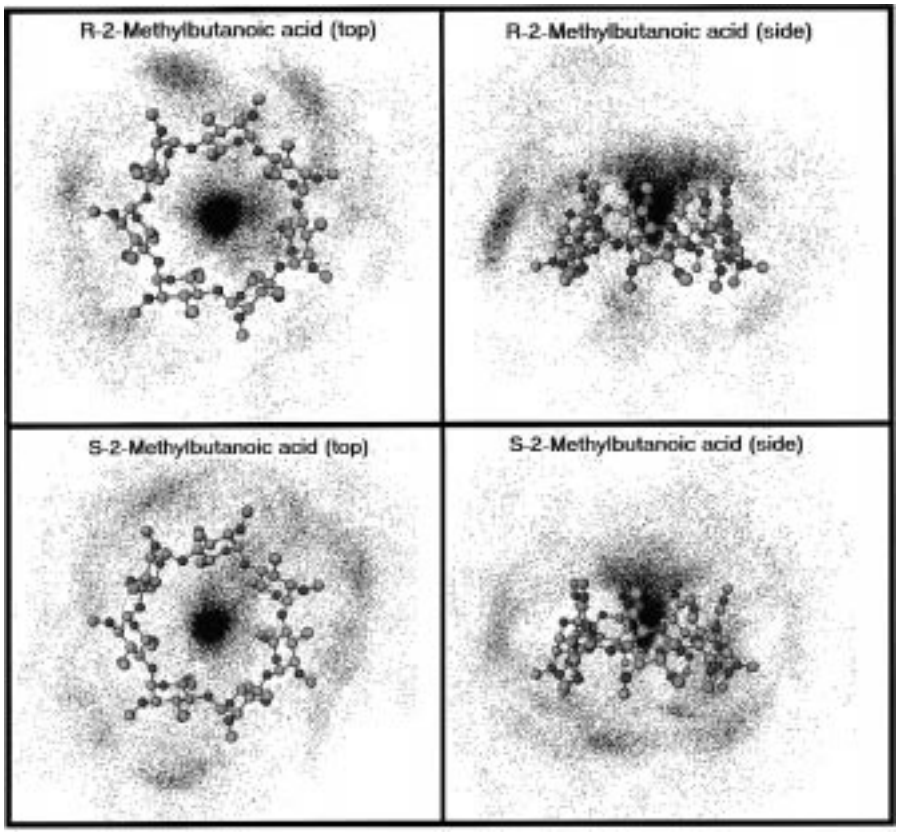

Figure 6. "Dot plot" illustrating the center of mass of guest **6**, relative to the cyclodextrin, over the combined 50 ns simulation. Top: end-on and side views of the *R* enantiomer. Bottom: end-on and side views of the *S*-enantiomer. Original diagrams are also color coded to indicate the intermolecular energy at each point. Lowest energies are at the interior.

Table 8. Trajectory-Averaged Intermolecular Energies for 4/CD

	R		*S*	
trajectory	vdW	elec	vdW	elec
I	−28.45	−2.78	−41.01	−3.35
II	−44.35	−4.48	−23.86	−2.97
III	−28.80	−3.35	−43.01	−4.37
IV	−26.32	−2.99	−25.99	−2.79
V	−42.54	−4.61	−43.33	−4.18
avg	**−33.09**	**−3.64**	**−35.44**	**−3.53**

Table 9. Trajectory-Averaged Intermolecular Energies for 5/CD

	R		*S*	
trajectory	vdW	elec	vdW	elec
I	−46.47	−7.12	−46.42	−7.69
II	−47.24	−7.57	−47.40	−6.58
III	−46.41	−7.36	−47.02	−7.55
IV	−12.02	−3.79	−34.06	−6.01
V	−44.84	−6.44	−47.28	−7.00
avg	**−39.40**	**−6.45**	**−44.44**	**−6.97**

combined and placed on a three-dimensional grid. The sides connecting eight adjacent grid points define a volume element. The number of guest positions in each volume element is tallied, and the resulting number densities are output in a form suitable for visualization with IRIS Explorer.[26] This allows us to identify where the guests prefer to bind to the CD (see below).

To determine regions of maximum enantiodifferentiation (see discussion later) we used an in-house program called

(26) IRIS Explorer Center (North America), Downers Grove, IL 60551-5702 or via <URL http://www.nag.co.uk/1h/Welcome_IEC>.

Table 10. Trajectory-Averaged Intermolecular Energies for 6/CD

	R		*S*	
trajectory	vdW	elec	vdW	elec
I	−23.48	−10.96	−21.12	−13.44
II	−17.79	−14.69	−18.46	−11.85
III	−20.34	−12.32	−17.09	−13.18
IV	−13.32	−15.66	−15.50	−13.32
V	−30.79	−12.55	−18.84	−13.18
avg	**−21.14**	**−13.24**	**−18.20**	**−12.93**

mmodgrid [27] running on an SGI computer. It is written in C language, parallelized, and available from one of the authors.[27] Among other features, this program allows one to carry out grid scans using different force fields. The AMBER* force field was used with an effective dielectric set to unity and without any cutoffs of any kind. Because of the nature of the systematic grid search being done, the software has been parallelized, and in this study we used simultaneously eight processors of a Cray J90 in addition to 15 available processors on various types of SGI workstations. The dimensions of the grid surrounding the cyclodextrin are 27 Å × 23 Å × 26 Å. We have selected grid spacings of 0.25 Å and 45° rotations per axis. Hence, at each grid point we sample 512 unique orientations of guest relative to host. The total number of grid points for the *R* and also for the *S* guest is approximately 269 000 each. Visualization of the results was done using IRIS Explorer as above.

(27) MMODGRID: written by M.A.P. to calculate intermolecular interaction energies along a grid using the AMBER* and MM3* force fields. This program is available from B. Coner: coner_bob@lilly. com. A parallel version, which uses the PVM library (PVM: Parallel Virtual Machine, MIT Press: Cambridge, 1994) is also available.

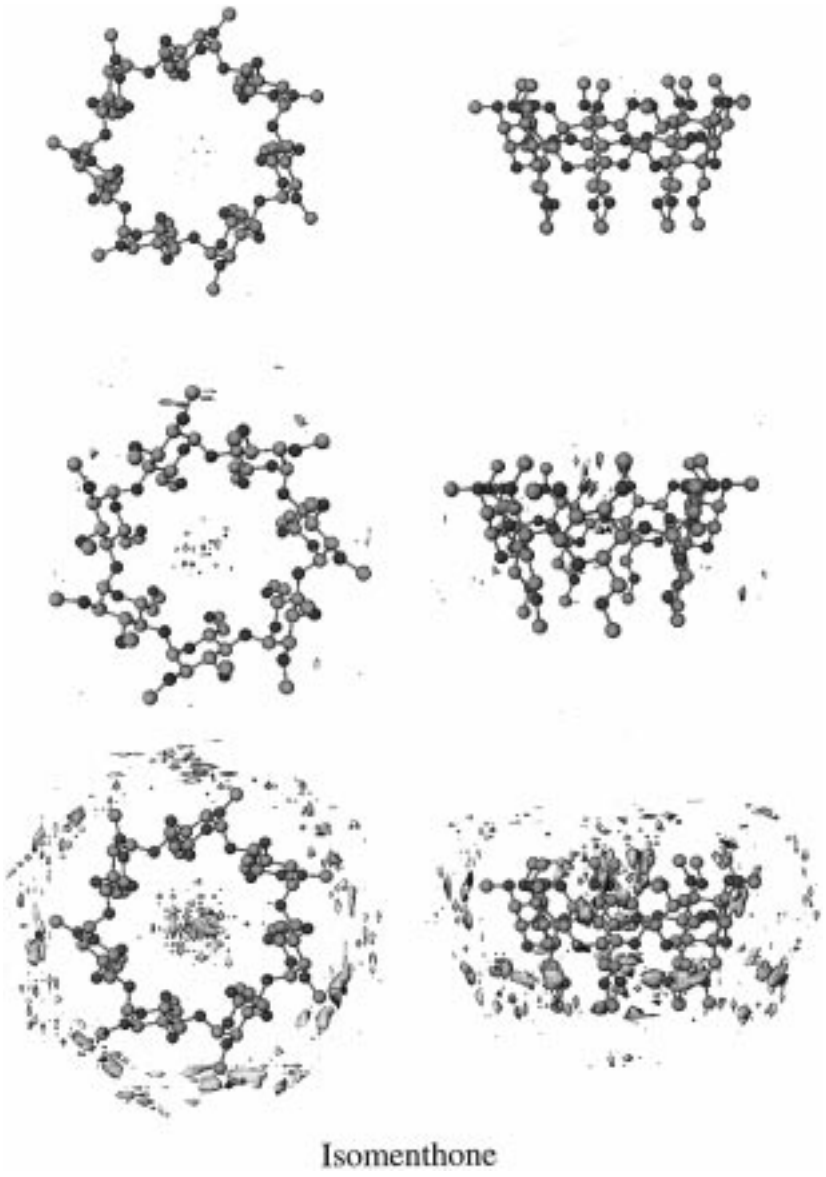

Figure 7. Regions of chiral recognition between a symmetric host, permethyl-β-cyclodextrin, and chiral probe **2**. The cyclodextrins and their gray-tone color codes are the same as in Figure 1. The most discriminating region is depicted at the top panel of the figure. Regions of less chiral discrimination are enclosed in the second panel, which shows that exterior sites are also discriminatory but to a lesser extent. Bottom panel show regions of space that are even less discriminatory than above. Inside the macrocycle the region of greatest discrimination is localized near the (wider) secondary rim. At all levels of chiral discrimination the inside of the macrocycle is most cognizant of differences between enantiomeric guests.

Results

The results of our molecular simulations are compiled in Tables 1−5. In these tables, the column heading "total" refers to the sum of the component force field energies computed by the AMBER* force field. The heading "stretch" refers to the compression/elongation energies for all bonds in the system averaged over a particular trajectory. Similarly the column heading "bend" refers to the bending energies of all bond angles in the system averaged over a given trajectory, and the term "torsion" refers to the corresponding dihedral angles around all bonds in the system. The "vdW" and "electrostatic" column headings refer to the short-range dispersion (van der Waals) and long-range electrostatic (Coulombic) components of the total energy, respectively. The row entries are labeled as R1, R2, etc., indicating trajectory no. 1 for the *R* enantiomer, trajectory no. 2 for the *R* enantiomer, and so on. Likewise, S1, S2, etc. refer to the corresponding trajectories for the *S* enantiomer. Note that in all cases each trajectory begins from the same initial location and with the same orientation as its mirror image. Also note that each trajectory is 5 ns in duration (25 ns total) with the exception of those for the phenylethanol and butanoic acid, which are 10 ns each (50 ns total). The reason for extending the simulation times for these analytes is that they contain hydroxyl and carboxylic acid moieties that were found to be more "sticky" than the others. By "sticky" we mean that each enantiomer tended to bind more tightly and for longer periods of time to a single oxygen atom on the host than did the other molecules, giving rise to a very nonuniform distribution of binding domains (after 5 ns). By remaining in one region around the cyclodextrin for extended time periods we were worried that these guests would not be sampling a large enough volume of phase space to provide thermodynamically meaningful results. To

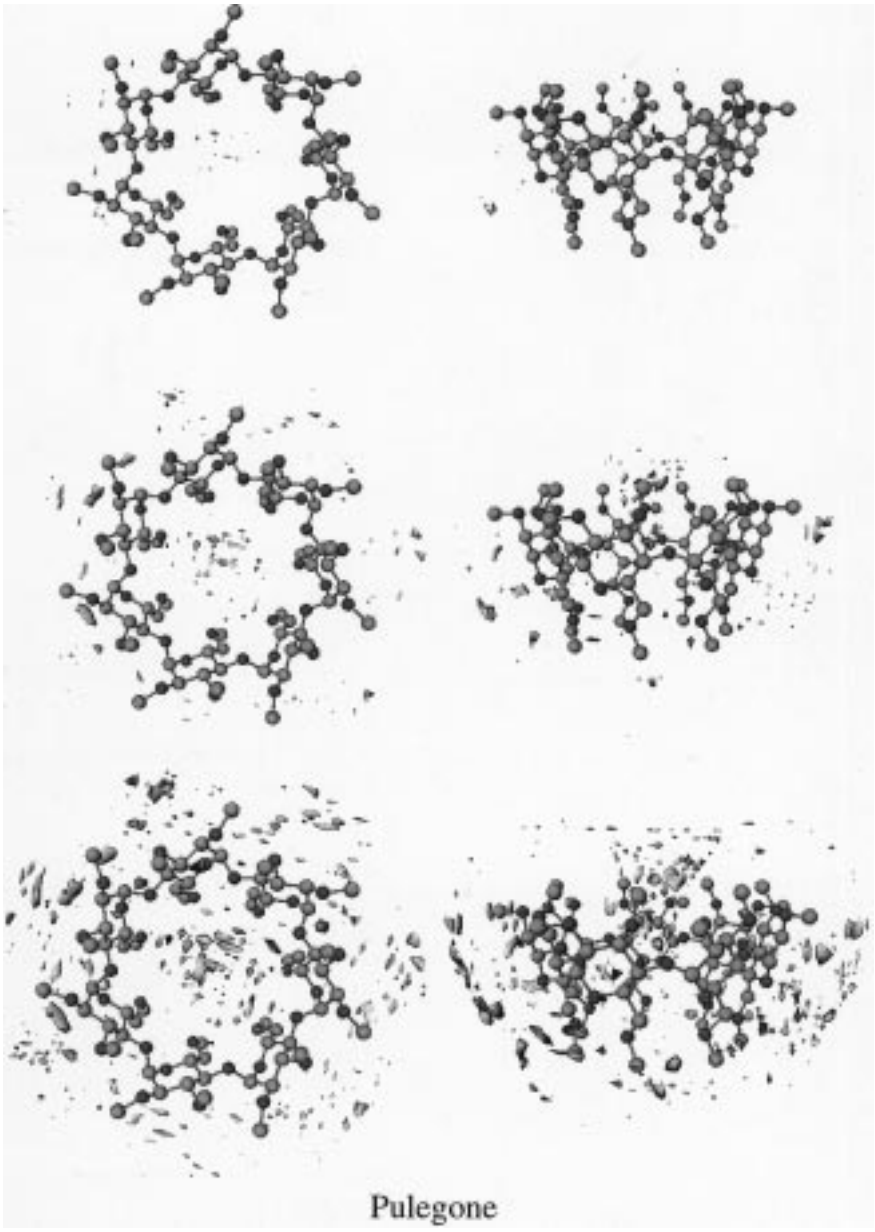

Figure 8. Same as in Figure 7 for guest **3**.

overcome this stickiness problem we simply ran the simulation for a longer time period, allowing the guest to better explore all binding regions in and around the CSP.

The results in these tables are consistent with the corresponding retention orders found experimentally,[17−20] and they are also consistent with the small enantioselective energy differences found experimentally. Accordingly, we feel confident in using the data from these simulations to begin answering the four questions posed above.

Discussion

In this section we begin extracting information from the simulations with the intention of answering those questions. The following subsections are presented in the order of those four questions to accomplish this goal.

(a) Guest Binding Sites. To answer the question of where the guest is most likely to be found, we placed the time-averaged CD's center of mass at the origin of a Cartesian coordinate system, which in turn was placed on a three-dimensional grid. Eight neighboring grid points constitute a small volume element that is called a "voxel" or a volumetric pixel. The number of times a guest's center of mass passed through a particular voxel, evaluated over the entire simulation time period, was tallied. The most densely populated volume elements are the preferred binding sites. To visualize this we present Figures 2−6 showing the locations of guests **2**−**6** over the course of the simulation.

Evident from these figures is that all guests prefer to bind to the interior of the CD cavity. The reason for this behavior is that interior binding is stabilized by the macrocycle, which collapses around these small guests, thus maximizing van der Waals forces (in contrast to exterior binding). One also notes, in general, that the more tightly bound substrates have better defined binding sites than do the less tightly bound enantiomers, which appear more scattered. It is also instructive to note that preference is given for all guests to bind to the

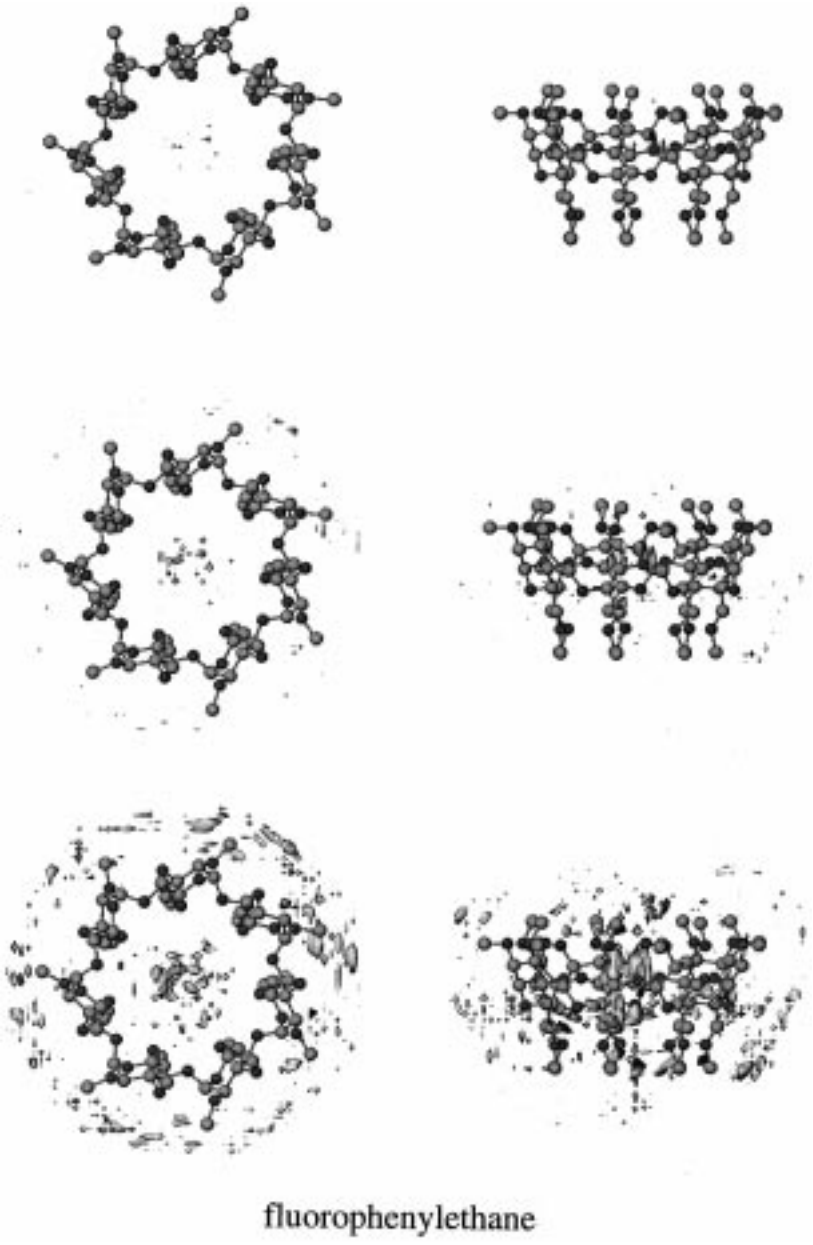

Figure 9. Same as in Figure 7 for guest **4**.

primary rim of the macrocycle, but this is difficult to discern in some cases. Generally, however, at these elevated gas chromatographic conditions the analyte is rapidly sliding back and forth between the two rims as well as into and out of the cavity itself. Clear preference is noted for interior binding rather than exterior binding, and there exists a propensity for analytes to associate with the more flexible primary rim of the cavity rather than the secondary rim.

(b) Forces Responsible for Complexation. The data in Tables 1−5 represent the total energies of the diastereomeric complexes. It is important to recognize that these data contain both intramolecular energies mixed together with intermolecular energies. The origin of this stems from the fact that the force field does not distinguish nonbonded atoms on one molecule (the host) from those on another molecule (the guest). To a force field a nonbonded interaction is the same irrespective of which molecule those atoms belong to. Hence, the van der Waals energies listed in Tables 1−5 include the following: (a) the van der Waals energies of the nonbonded atoms on the cyclodextrin interacting with other nonbonded atoms on the cyclodextrin, (b) the van der Waals energy of the analyte interacting with itself in a similar way, and (c) the van der Waals energy of all the analyte atoms interacting with all the cyclodextrin's atoms. The same is true for the electrostatic energies in Tables 1−5. Most computer programs provide only the total energies as in Tables 1−5. However, we have written a program that projects out only the intermolecular energies between the host and guest molecules. This is useful because these energies inform us about the types of intermolecular forces contributing to the complexation energy as well as their magnitudes. These intermolecular energies are compiled in Tables 6−10. Note that the only intermolecular energies involved are the nonbonding terms (van der Waals and Coulomb energies) because there exists no bond stretching, angle bending, etc., between a host and a guest that are not covalently linked.

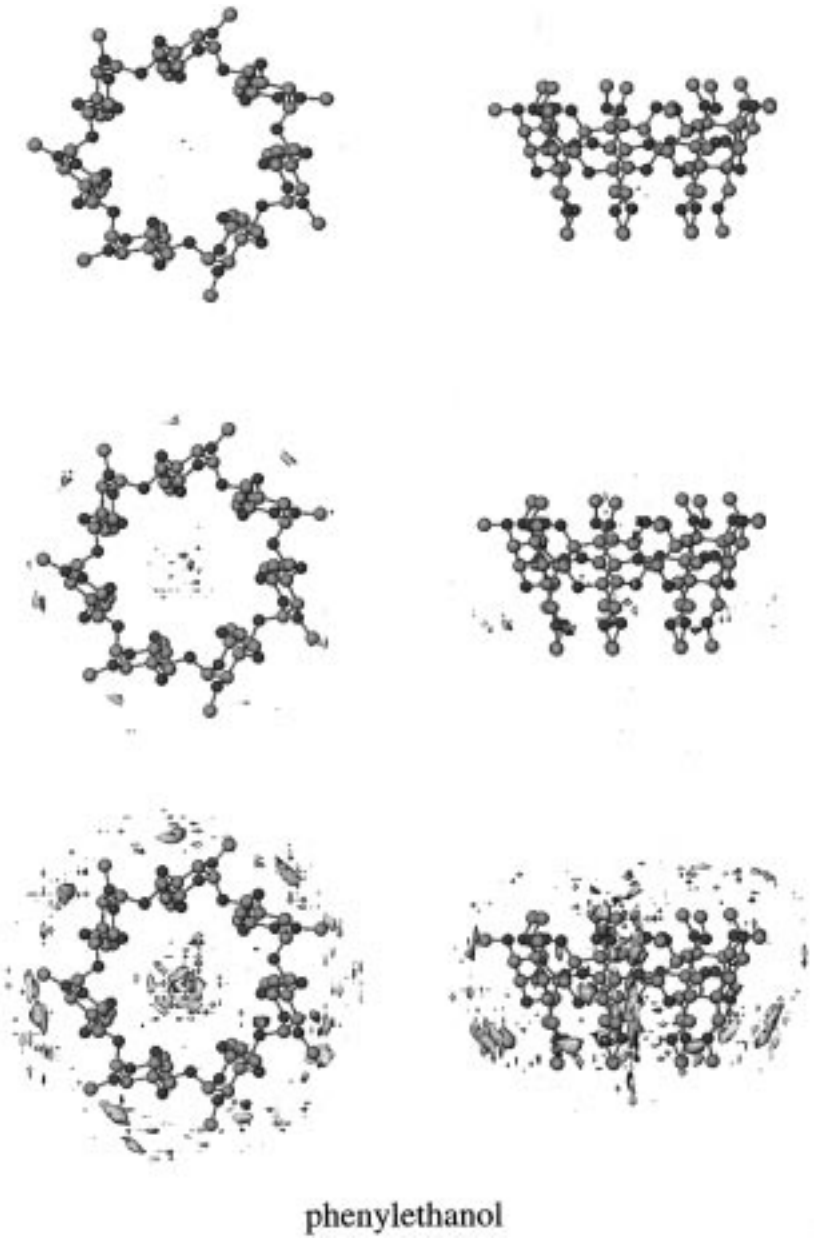

Figure 10. Same as in Figure 7 for guest **5**.

It is anticipated (and found) that all of the intermolecular energies on average (as well as for all individual trajectories) have negative values. This means the intermolecular interactions are overall attractive. Moreover, we find that the electrostatic and the van der Waals terms are both attractive. It is possible to find a situation where one force is attractive while the other is repulsive, but in the examples presented in this study (and using this force field) both are contributing in an attractive way to the host−guest binding. In terms of answering the question "Which forces are most responsible for host−guest binding?" we note that in all cases the van der Waals contributions in Tables 6−10 dominate. It is instructive to consider each guest in turn.

The analytes **2**−**4** contain moderately polar C−F and C═O functionality. These functional groups can associate with the comparably polar C−O bond moments of the cyclodextrin by dipole−dipole interactions. The remaining portion of those analytes contains hydrocarbon fragments having even smaller bond dipoles, and accordingly, for these molecules one would anticipate most of the intramolecular energies to arise from van der Waals forces. Analytes **5** and **6** each have a hydroxylic or carboxylic O−H group that can hydrogen bond to the cyclodextrin's oxygen atoms. Hydrogen bonds are mainly electrostatic in nature, so we anticipate that these analytes will have a larger contribution from the electrostatic force than do guests **2**−**4**. But, because these molecules are mostly hydrocarbons, the net intermolecular force should still be dominated by the van der Waals attractive terms.

These intuitive predictions are exactly what one finds from the molecular simulations. The advantage of the simulation, though, is that one can quantify exactly how much of the intermolecular force is attributed to each term. When the *RR* isomer of isomenthone, **2**, binds to host **1**, the van der Waals contribution is 84.0% and the Coulomb contribution is 16%. When the *SS* isomer binds we find 81.7% attributed to van der Waals forces and 18.3% from electrostatics. When the *R* enantiomer of

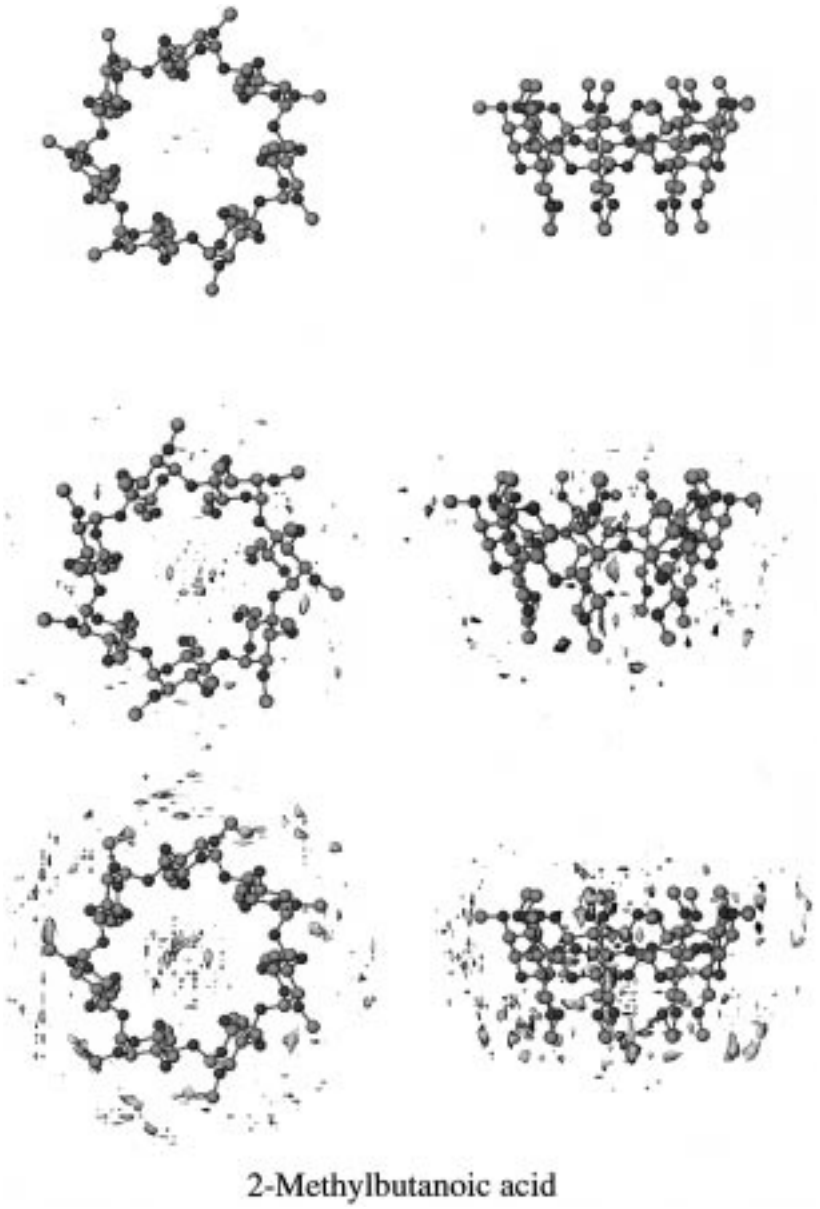

Figure 11. Same as in Figure 7 for guest **6**.

pulegone binds, the van der Waals contribution is 89.3% and the electrostatic contribution is 10.7%. When (*S*)-pulegone binds the van der Waals contribution is 91.4% and the electrostatic contribution is 8.6%. When the *R* enantiomer of 1-fluoro-1-phenylethane binds, the van der Waals contribution is 90.1% and the electrostatic contribution is 9.9%; when the *S* enantiomer binds the values are 90.9% and 9.1%, respectively. The large domination of van der Waals forces is to be expected for these weakly polar molecules containing so much hydrocarbon content.

When the *R* enantiomer of 1-phenylethanol binds we find 85.9% van der Waals contribution and 14.1% Coulomb contribution; when its mirror image binds the corresponding values are 86.4% and 13.5%. Finally, for the highly acidic guest **6** we see that when the *R* analyte binds, 61.49% of the intermolecular attraction arises from the van der Waals term while 38.51% comes from electrostatics. For the antipode of **6** the values are 58.46% and 41.54%, respectively. Hence, irrespective of the chirality of the guest, in all cases studied here the major contributor to the intermolecular force leading to host−guest complexation is the short-range van der Waals force. We note, though, that as the guests' chemical functionality becomes more polarized or more acidic that the relative contributions from Colombic forces become more important. Indeed, on the basis of this one would predict that small dicarboxylic acids (if not self-associating) will be dominated by electrostatic rather than van der Waals interactions when interacting with the cyclodextrin.

(c) Forces Responsible for Chiral Recognition. While the forces responsible for holding the binary complexes together are primarily the van der Waals forces, there is no basis for predicting, *a priori*, which intermolecular force is responsible for chiral discrimination. To determine this, we evaluate the *differential* intermolecular forces for each enantiomer in the field of its host cyclodextrin; i.e., we compare the averaged intermolecular van der Waals energies for the *R* enantiomer compared with the *S* enantiomer in Tables 6−10 and determine if those energy differences are greater or smaller in magnitude than the corresponding electro-

static values. For example, in Table 6 the average intermolecular van der Waals energy difference, $\Delta\Delta E_{vdw}$, is 1.46 kJ/mol (−25.14 vs −23.68) and the differential electrostatic value, $\Delta\Delta E_{elec}$, is 1.12 kJ/mol (−5.64 vs 4.52). Likewise for analyte **3** we find $\Delta\Delta E_{vdw} = 1.02$ kJ/mol and $\Delta\Delta E_{elec} = 0.27$ kJ/mol. For analyte **4** we find $\Delta\Delta E_{vdw} = 2.35$ kJ/mol and $\Delta\Delta E_{elec} = 0.11$ kJ/mol. For analyte **5** we find $\Delta\Delta E_{vdw} = 5.04$ kJ/mol and $\Delta\Delta E_{elec} = 0.52$ kJ/mol. Finally, for analyte **6** we find $\Delta\Delta E_{vdw} = 2.94$ kJ/mol and $\Delta\Delta E_{elec} = 0.31$ kJ/mol. In all cases, the larger differences exist in the van der Waals forces so we conclude that the most enantiodifferentiating forces are the van der Waals forces. Hence, the same forces responsible for host−guest complexation are also most responsible for chiral discrimination.

(d) Regions of Greatest Chiral Discrimination. Knowing where guests tend to bind in or around a cyclodextrin is important, but this aspect of molecular recognition constitutes only part of what leads to effective chiral recognition. Another aspect that is critical for effective resolutions is knowing which region of the CSP is most discriminating. This is especially important because if the preferred binding site differs from the site that is most highly discriminating one is relegated to an inferior region of chiral selection leading to loss of discriminatory power or even no recognition at all. This aspect of chiral recognition is what we will refer to as "the principle of maximum chiral recognition", which states that maximum chiral recognition is assured when the guest's binding site and the host's most enantiodiscriminating region are spatially coincident. This is an intuitive and seemingly trivial concept in some ways, but in other ways it is a profound concept that appears not to have been discussed in the literature. Having a priori knowledge of which region of a host is most discriminatory is especially useful because one could then devise techniques to force the substrate to bind to a thermodynamically less-favored but more discriminatory site. In terms of chiral chromatography with, say, cyclodextrins, this could be as simple as adding to the mobile phase a competing substrate that binds exclusively to the interior of the cyclodextrin, thus forcing the guest to the less favored and (possibly) more discriminating exterior of the cyclodextrin. This would first reduce the retention time of the analytes on the column and second enhance the resolution, both of which are desirable traits in chromatography, but the concept can be generalized to any other situation where chiral recognition is important.

Although we have located the preferred binding site (inside the cyclodextrin cavity) and we were able to define the intermolecular forces responsible for both complexation and molecular recognition (dispersion forces) we have not identified the most discriminating regions of the host molecule. To do this, we adopt the following procedure. The time-averaged, 7-fold symmetric cyclodextrin's center of mass is placed at the origin of a Cartesian coordinate system and a uniform grid is placed over that coordinate system. At each grid point the guest's center of mass is positioned and then systematically rotated about a local coordinate system along three orthogonal axes. The number of grid points and the number of rotations per axis is arbitrary, but we use 512 unique orientations per guest at each grid point (see computational tools section). Rather than saving only the lowest energy orientation at each grid point we Boltzmann average the energies at each grid point. Because we are using a deterministic grid search methodology we note that whatever is being done to the *R* enantiomer is being done equivalently to the *S* enantiomer; this way sampling artifacts are removed. The differences at each grid point, between *R* vs *S* guests, indicate discriminatory regions. Those grid points with zero or small energy differences between mirror image isomers are not discriminating, while those grid points with the largest differences are most discriminating.

The results of our calculations show that the greatest difference in interaction energy for *R* vs *S* probes exists in the interior of the macrocycle as illustrated in Figures 7−11. In these figures are plotted isoenergy contour surfaces of *differences* in Boltzmann-weighted energies between *R* and *S* probe molecules at each grid point. At the top of each figure is the region of greatest energy difference and is thus the most enantiodiscriminating part of the CSP. In the next two panels of each figure are regions containing smaller and smaller differential energies, which in turn are encompassing volumes of space having less and less enantiodiscrimination. Of course, the regions not being rendered are very weakly discriminating or have no chiral recognition at all (at least for that particular probe).

What we find, then, is that the most enantiodifferentiating region of the macrocycle (the interior) is also where the analytes prefer to bind. So, in this case of molecular recognition Nature places the analytes in the vicinity of highest chiral discrimination. On the basis of the spatial congruence of the analyte binding site with the host's regions of maximum enantiodifferentiation we can now see why permethyated β-cyclodextrin is such a useful chiral stationary phase.

Summary

To help answer the question "How does permethyl-β-cyclodextrin work as a chiral stationary phase in gas chromatography?" we posed and answered four important questions. By addressing those questions we conclude the following: (1) Analyte molecules tend to bind to the interior of the cyclodextrin's cavity with a slight preference for the primary rim. Binding to the interior leads to a stabilization of intermolecular attraction by way of cyclodextrin collapse around the analyte. Nonetheless, the guest molecules can quickly escape from the interior of this cavity, especially at such elevated temperatures. (2) The dominant intermolecular force responsible for host−guest coordination is the short-range dispersion force rather than the long-range electrostatic force. As the polarity of functional groups on the guest increase one expects and finds more of a contribution from the electrostatic part of the intermolecular force. Usually, however, this electrostatic force is overshadowed by the dispersion forces arising from the remaining hydrocarbon part of the guest. (3) The intermolecular force most responsible for enantiodifferentiation is also the short-range dispersion force. (4) The region of maximum enantiodifferentiation is found, for the molecules studied in this paper using the AMBER* empirical force field, to be the interior of the cyclodextrin. Although enantioselective regions exist both outside and inside of the macrocycle, the interior is more discriminatory.

In summary, the molecular simulations carried out in this study have illuminated not only how permethyl-β-cyclodextrins work, but also where they work most

effectively. From these results we can also begin to appreciate why this particular cyclodextrin is such a good CSP for chromatographic resolutions: essentially, Nature places the analyte in the region of the cyclodextrin that is most enantiodifferentiating. The concept of maintaining spatial coincidence between the host's region of maximum enantiodifferentiation and the preferred site of guest binding was presented here. This concept is seemingly trivial but is profoundly significant when one wants to maximize chiral recognition and we urge other scientists to consider this aspect of molecular recognition in their studies.

Acknowledgment. This work was sponsored by a grant from the National Science Foundation (CHE94-12512).

JO9717090